Chapter 24
Cartographic Mapping of the Icy Satellites Using ISS and VIMS Data

Th. Roatsch, R. Jaumann, K. Stephan, and P.C. Thomas

Abstract The sizes and shapes of six icy Saturnian satellites have been measured from Cassini Imaging Science Subsystem (ISS) data, employing limb coordinates and stereogrammetric control points. Mimas, Enceladus, Tethys, Dione and Rhea are well described by triaxial ellipsoids; Iapetus is best represented by an oblate spheroid. The ISS acquired many high-resolution images (<1 km/pixel) during close flybys of the medium-sized icy Saturnian satellites (Mimas, Enceladus, Tethys, Dione, Rhea, Iapetus, and Phoebe). We combined these images with lower-resolution coverage and a few images taken by Voyager cameras to produce high-resolution mosaics of these satellites. The global mosaics are the baseline for high-resolution atlases. The atlases consist of 15 tiles each for Enceladus, Dione, and Tethys, whereas the Iapetus, Mimas, and Phoebe atlases consist of 3, 1, and 1 tile, respectively. The nomenclature used in these atlases was suggested by the Cassini-ISS team and approved by the International Astronomical Union (IAU). The whole atlases are available to the public through the Imaging Team's website (http://ciclops.org/maps/) and from the Planetary Data System (PDS, http://pds-imaging.jpl.nasa.gov/). Additionally to ISS, the Visual and Infrared Mapping Spectrometer (VIMS) onboard the Cassini spacecraft detected the chemical and physical surface properties of the Saturnian satellites. Multiple VIMS observations were combined into global VIMS maps representing the VIMS coverage achieved during the nominal Cassini mission. Progressed mapping has been done for the satellites Dione, Rhea, and Enceladus.

24.1 Introduction

The Cassini Imaging Science Subsystem (ISS) consists of two framing cameras. The narrow angle camera is a reflecting telescope with a focal length of 2,000 mm and a field of view of 0.35°. The wide angle camera is a refractor with a focal length of 200 mm and a field of view of 3.5°. Each camera is outfitted with a large number of spectral filters which, taken together, span the electromagnetic spectrum from 0.2 to 1.1 μm. At the heart of each camera is a charged coupled device (CCD) detector consisting of a 1,024 square array of pixels, each 12 microns on a side. The data system allows many options for data collection, including choices for on-chip summing and data compression. The stated objective of the ISS is to obtain global coverage for all medium-sized icy satellites with a resolution better than 1 km/pixel and high-resolution images of selected areas (Porco et al. 2004). This goal was achieved with image sequences obtained during close flybys supplemented by images from greater distances to complete the coverage. Close flybys of all medium sized satellites except Mimas were executed during the nominal mission of the Cassini spacecraft. The first flybys during the mission were those of Phoebe in June 2004 and Iapetus in December 2004 followed by three flybys of Enceladus in February, March, and July 2005 (Porco et al. 2005, 2006).

As an imaging spectrometer the Visual Infrared Mapping Spectrometer (VIMS) onboard the Cassini spacecraft combines the characteristics of both a spectrometer and an imaging instrument. This makes it possible to analyze the spectrum of each pixel separately and to map the spectral characteristics spatially, which is important to study the relationships between the spectral information and geological and/or geomorphological surface features. VIMS operates in a spectral range from 0.35 to 5.2 μm generating spectral image cubes in which each pixel represents a spectrum of 352 contiguous wavebands (Brown et al. 2004). It is the first imaging spectrometer operating in the Saturnian system and providing spectral data with sufficient pixel ground resolution up to 2 km/pixel. This allows the mapping of spectral variations related to physical and chemical surface properties across the satellites surfaces that could be combined into composition maps of a specific satellite.

In this work we first review in Section 24.2 the method of shape determination and evaluation for the icy satellites, followed by reporting the measurement results for the satellites. We then examine how close each moon is to an equilibrium

Th. Roatsch, R. Jaumann, and K. Stephan
Institute of Planetary Research, German Aerospace Center (DLR), 12489 Berlin, Germany

P.C. Thomas
Center for Radiophysics and Space Research, Cornell University, Ithaca, NY 14853, USA

M.K. Dougherty et al. (eds.), *Saturn from Cassini-Huygens*,
DOI 10.1007/978-1-4020-9217-6_24,

shape. Then we view the results in total, and finally evaluate the significance of departures from equilibrium forms. Details of the image processing that is necessary to generate the global mosaics of the medium-sized satellites are described in Section 24.3. Section 24.4 summarizes the cartographic work that produced our high-resolution atlas. During Cassini's nominal tour VIMS was able to observe especially the Saturnian satellites Dione and Enceladus with sufficient pixel ground resolution and signal-to-noise ratio (SNR) to combine the VIMS results into regional and global maps as described in Section 24.5. The final section describes our plans for the extended mission.

24.2 Shapes and Sizes of the Saturnian Satellites

The shapes and sizes of the icy Saturnian satellites, required for mapping and global geophysical interpretations, are derived primarily by limb profile analysis for the ellipsoidal satellites (Mimas, Enceladus, Tethys, Dione, Rhea, and Iapetus) and by stereo control points and limb matching for the smaller, irregularly-shaped ones. Limb analysis is described in Thomas et al. (1998); small satellite shape modeling in Simonelli et al. (1993).

Images suitable for limb analysis are full-disk with phase angles $<85°$, plus higher phase images in which part of the solar-shadowed region has sufficient Saturn shine for measurement. Transits of a satellite across the illuminated disk of Saturn provide the best measurements, essentially full disk limb data. Limb measurement can be made with precisions of order 0.1 pixels, but in practical terms the roughness of the limb limits center-fixing accuracy, hence the accuracy of the calculated shape. Greater geographical distribution of the limb tracks enhances the accuracy of the solution. A rough object such as Tethys can yield very different triaxial solutions with only a few ground tracks, then the results of the fit usually stabilize as more profiles are added. The progressive refinement of the shape solution of Tethys with increasing image coverage is shown in Fig. 24.1. Portions of limbs can provide some information about local topography, such as large crater depth profiles, rim profiles, and relief on suitably aligned scarps.

The Cassini results greatly improved the Voyager data. Dione and Rhea's mean radii were uncertain to several km, Iapetus' shape and mean radius have improved drastically (more than 10 km) and the shapes of Enceladus and Mimas are sufficiently refined to change interpretations. The small satellites were only approximately measured prior to Cassini data.

Shapes are useful in scientific interpretation as well as for cartographic work. Among the ellipsoidal satellites, the most revealing shape is that of Iapetus. As noted by Castillo et al. (2007), the oblate spheroid shape of this object indicates a frozen figure from a time of more rapid spin ($\sim$16 h period). Subsequent limb data have only strengthened the conclusion that this oblate form represents a fossil bulge from rapid rotation.

The shapes of the other satellites all come close to those of equilibrium, effectively fluid, ellipsoids. In Tables 24.1 and 24.2 we list the derived global properties, one of which, $F = (b - c) / (a - c)$ can be an indicator of how close to an equilibrium shape (here assumed fluid equilibrium) the object is. The observed values of F and the predicted ones are also listed in Table 24.2. The predicted values of F decrease slightly for the very fast rotating satellites (Chandrasekhar 1969; Dermott and Thomas 1988). While many of the observed F values are close to the ideal 0.25–0.21, only Tethys and Dione actually satisfy the relationship at the measurement uncertainty. Yet the data, and the smoothness of limb topography (Thomas et al. 2007) suggest all these objects have approached equilibrium forms.

The chief scientific interest is in the modest departures from the idealized shapes. For instance, while Enceladus' F parameter is fractionally quite distinct from the theoretical value, it in fact represents less than 2 km deviation from that ideal. The (a–c) value for Enceladus is appropriate for

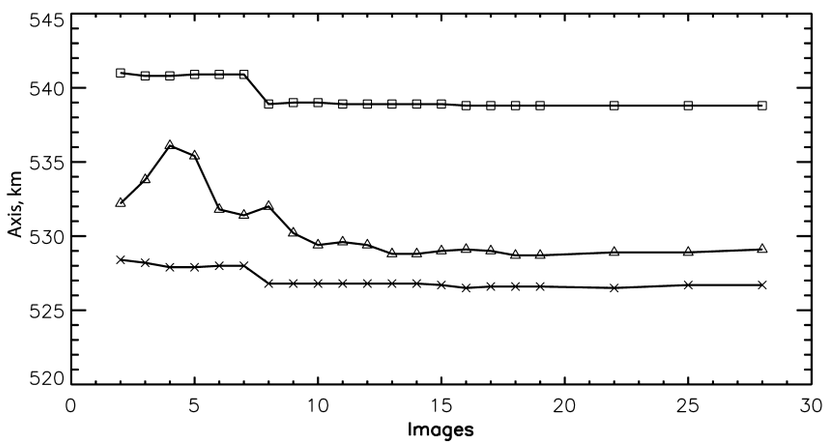

Fig. 24.1 Tethys axial fits with increasing number of images

Table 24.1 Satellite shapes from limb data

Satellite	a	b	c	Mean radius	a–c	im	Data
Mimas	207.8 ± 0.5	196.7 ± 0.5	190.6 ± 0.3	198.2 ± 0.4	17.2 ± 0.5	36	21,527
Enceladus	256.6 ± 0.6	251.4 ± 0.2	248.3 ± 0.2	252.1 ± 0.2	8.3 ± 0.6	34	23,226
Tethys	538.4 ± 0.3	528.7 ± 1.7	526.3 ± 0.6	531.1 ± 0.6	12.1 ± 0.9	28	18,128
Dione	563.4 ± 0.6	561.3 ± 0.5	559.6 ± 0.4	561.4 ± 0.4	3.8 ± 0.7	43	33,229
Rhea	766.2 ± 0.6	762.8 ± 1.0	762.4 ± 1.2	763.8 ± 1.0	3.8 ± 1.1	38	29,606
Iapetus	746.0 ± 2.9	746.0 ± 2.9	712.0 ± 1.6	734.5 ± 2.8	34.0 ± 3.6	51	14,607

Here we use a–c (all in km) to denote the Saturn-facing, orbit-facing, and polar radii. im: number of images used; data: number of data points.

Table 24.2 Satellite shape parameters

Satellite	Mean radius (km)	ρ (kg/m^3)	a–c (km)	(a–c)h (km)	F_{obs}	F_{pred}
Mimas	198.2 ± 0.4	1,149 ± 7	17.2 ± 0.6	19.7	0.35 ± .02	0.21
Enceladus	252.1 ± 0.2	1,609 ± 5	8.3 ± 0.6	8.0	0.37 ± 0.04	0.23
Tethys	531.1 ± 0.6	984 ± 3	12.1 ± 0.9	14.7	0.28 ± 0.20	0.24
Dione	561.4 ± 0.4	1,478 ± 3	3.8 ± 1.2	4.9	0.20 ± 0.37	0.25
Rhea	763.8 ± 1.0	1,236 ± 5	3.8 ± 1.5	2.9	0.05 ± 0.20	0.25
Iapetus	734.5 ± 2.8	1,088 ± 13	34.0 ± 3.6	0.01	n/a	0.25

ρ, mean density, determined from masses reported in Jacobson et al. (2006).
(a–c) h is predicted (a–c) for homogeneous model.

Table 24.3 Sizes of irregularly-shaped Saturnian satellites

Satellite	A	B	C	Mean radius	Mass	ρ
Pa	17.4 ± 2.0	15.8 ± 1.3	10.4 ± 0.84	14.2 ± 1.3	0.495 ± .075	410 ± 150
Daphni	4.5 ± 0.8	4.3 ± 0.8	3.1 ± 0.9	3.9 ± 0.8	0.0077 ± 0.0015	310 ± 200
Atla	20.9 ± 1.4	18.1 ± 2.5	8.9 ± 0.8	15.1 ± 1.4	0.66 ± 0.06	440 ± 190
Prometheus	67.1 ± 3.0	39.6 ± 3.0	30.0 ± 1.8	43.1 ± 2.6	15.68 ± 0.20	470 ± 90
Pandora	52.1 ± 1.8	40.6 ± 2.0	32.0 ± 0.9	40.7 ± 1.5	13.58 ± 0.23	480 ± 60
Epimetheus	62.6 ± 1.5	54.9 ± 2.4	51.4 ± 0.7	56.8 ± 1.6	53.10 ± 0.14	690 ± 130
Janus	100.3 ± 1.7	94.7 ± 1.0	76.1 ± 1.1	89.8 ± 1.4	191.37 ± 0.005	640 ± 64
Methone	1.6 ± 0.6	1.6 ± 0.6	1.6 ± 0.6	1.6 ± 0.6		
Pallene	2.6 ± 0.4	2.2 ± 0.3	1.8 ± 0.2	2.2 ± 0.3		
Telesto	15.8 ± 0.6	11.7 ± 0.3	10.2 ± 0.3	12.3 ± 0.4		–
Calypso	15.0 ± 0.3	11.5 ± 2.3	7 ± 0.6	10.6 ± 0.7		–
Polydeuces	1.5 ± 0.6	1.2 ± 0.4	1.0 ± 0.2	1.3 ± 0.4		
Helene	19.4 ± 0.2	18.5 ± 1.0	12.3 ± 1.0	16.5 ± 0.6		
Hyperion	–	–	–	135 ± 4	561.99 ± 5	544 ± 50
Phoebe	107.7 ± 1.1	108.6 ± 2.3	101.5 ± 0.4	106.6 ± 1	829.2 ± 1	1,629 ± 50

Radii a–c are given in km, Mass in 10^{19}g and density in kg/m^3.
Size data have been updated from Porco et al. (2007) for Prometheus, Pandora, Epimetheus, and Janus. Mean radii are from shape models and may differ slightly from calculations using the ellipsoidal axis fits. Masses, in units of 10^{19} g, are those reported in Porco et al. (2007) from different sources.

a homogeneous equilibrium body. However, the overwhelming expectation (Porco et al. 2006) is that the interior has had enough heating to allow substantial segregation of materials and thus a simple onion layer model will leave the observed surface departing from an equipotential. The solution presumably involves lateral changes in crustal density, topography on any core, or lateral changes in mantle properties.

Rhea's shape also suggests it is not a highly differentiated, relaxed object.

The more irregularly shaped, smaller bodies may represent effects of accretion or effects of overlapping large impacts or even complete disruption. Apart from Atlas and Pan, none show strong signs of accretionary remnants. Atlas and Pan have smoother, equatorial bulges, which may reflect interactions with ring particles after the ring system collapsed to its present small thickness (Porco et al. 2007; Charnoz et al. 2007). It has been found that complex figures can be supported by unconsolidated bodies with characteristics of a "sand pile", which may play a role in some small object shapes (Minton 2008). Telesto has considerable regolith filling of craters, but it does not affect the overall shape and its regolith appears to be undergoing active downslope motion. Phoebe's shape is more equidimensional than most irregular satellites, but the range of topography relative to estimated equipotentials (28 km) and the obvious topographic effects of large craters indicates this object does not show significant effects of global viscous relaxation (Porco et al. 2005) (Table 24.3).

24.3 Global Basemaps Derived from Cassini-ISS Images

24.3.1 Data Processing

Though the Cassini-ISS camera takes images using many different filters (Porco et al. 2004), we used only images taken with the filters CL1, CL2 or GRN, as these images show similar contrast. The processing of the Cassini images follows the typical processing chain for framing cameras: radiometric correction, geometric correction and map projection, and mosaicking (Roatsch et al. 2006). For the Cassini mission, spacecraft position and camera pointing data are available in the form of SPICE kernels (http://naif.jpl.nasa.gov). While the orbit information is sufficiently accurate to be used directly for mapping purposes, the pointing information must be corrected using limb fits (Roatsch et al. 2006) or least-squares adjustment methods if enough stereo data are available as for Enceladus (Roatsch et al. 2008a). High-resolution images that do not contain the limb were registered to limb images to improve the pointing.

24.3.2 Coordinate System

The coordinate system adopted by the Cassini mission for satellite mapping is the IAU "planetographic" system, consisting of planetographic latitude and positive West longitude. The surface position of the prime meridians are defined by Davies and Katayama (1983a–c, 1984) and adopted by the IAU cartography working group as standard (Seidelmann et al. 2007) are defined by small craters. Our mosaics that were calculated using rotational parameters derived from Voyager data and the limb-fitted attitude data or the attitude data that were improved using a least-squares adjustment had a slight offset to this definition. Therefore we decided to shift the whole mosaics to be consistent with the IAU longitude definition. This requires also an update of the rotational parameters, which are used for the calculation of the prime meridian location, the so called rotational parameter W_0 (Seidelmann et al. 2007). Table 24.4 summarizes the reference craters, the necessary shift and the new values for W_0.

Table 24.4 New values of rotational parameter W_0

Satellite	Reference crater	Longitude shift (West)	W_0
Mimas	Palomides	−4.0	333.46
Enceladus	Salih	3.5	6.32
Tethys	Arete	−1.5	8.95
Dione	Palimurus	0.6	357.6
Rhea	Tore	0	235.16
Iapetus	Almeric	5.0	355.2

24.3.3 Basemaps

Digital global mosaics that are also called basemaps were prepared in simple cylindrical projection, a special case of equirectangular projection. The mapping cylinder is tangent to the equator of the sphere, the longitude range is 0°–360° W and latitude range –90° to 90° (Kirk et al. 1998). The prime meridian is in the center of the map. All basemaps were calculated using Cassini images. Voyager images were used to fill remaining gaps. The only exception is the Rhea basemap that is still based on Voyager data (Roatsch et al. 2006) overlayed by higher-resolution Cassini images. The calculation of a Cassini based Rhea basemap will be part of our future work.

Figures 24.2–24.8 show the basemaps of the medium sized satellites. We marked the most prominent features with their names. Some features were already named based on the Voyager images. Many new feature names were suggested by the Cassini imaging time and approved by the IAU. New Cassini based feature names are not yet available for Rhea. In naming the features on the Saturnian satellites, the Working Group for Planetary System Nomenclature within the International Astronomical Union (IAU) has expanded the mythological theme first used on the Jovian satellites. On the Saturnian satellites, however, the features bear names derived from the great epics and legends of the world (Batson 1984; http://planetarynames.wr.usgs.gov/). A summary of the epics used for feature names in the Saturnian system is given in Table 24.5.

24.4 High-Resolution Atlases

High-resolution atlases were produced to conform to the design and standards of the USGS airbrush maps and photomosaics, established by Greeley (1990), widely used in planetary cartography. The selection of the atlas format depends on the resolution of the mosaics and the size of the satellites. Three different formats were used for the generation of the atlases (Figs. 24.9–24.11):

- Synoptic format for making planetwide maps on a single sheet, used for Phoebe and Mimas (Roatsch et al. 2006, 2009)
- Subdivision of the synoptic format for making planetwide maps with four quadrangles on three sheets, used for Iapetus (Roatsch et al. 2009)

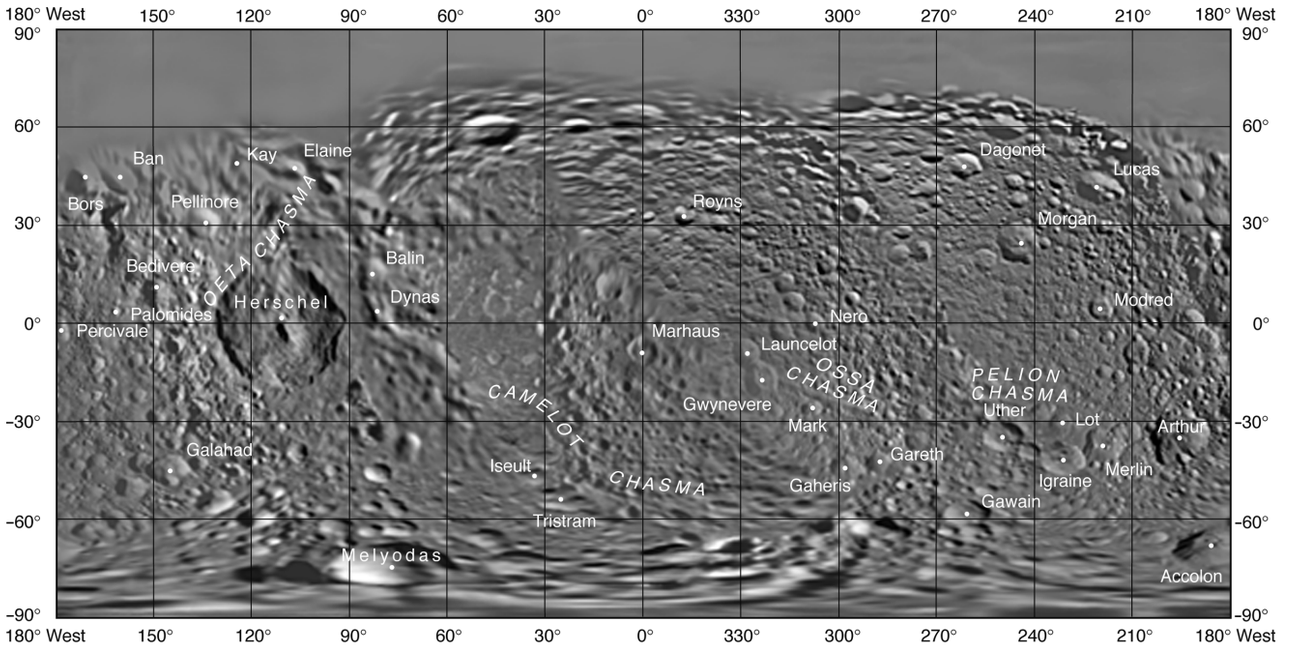

Fig. 24.2 Global mosaic of Mimas. The map exhibits a map scale of 0.43 km/pixel

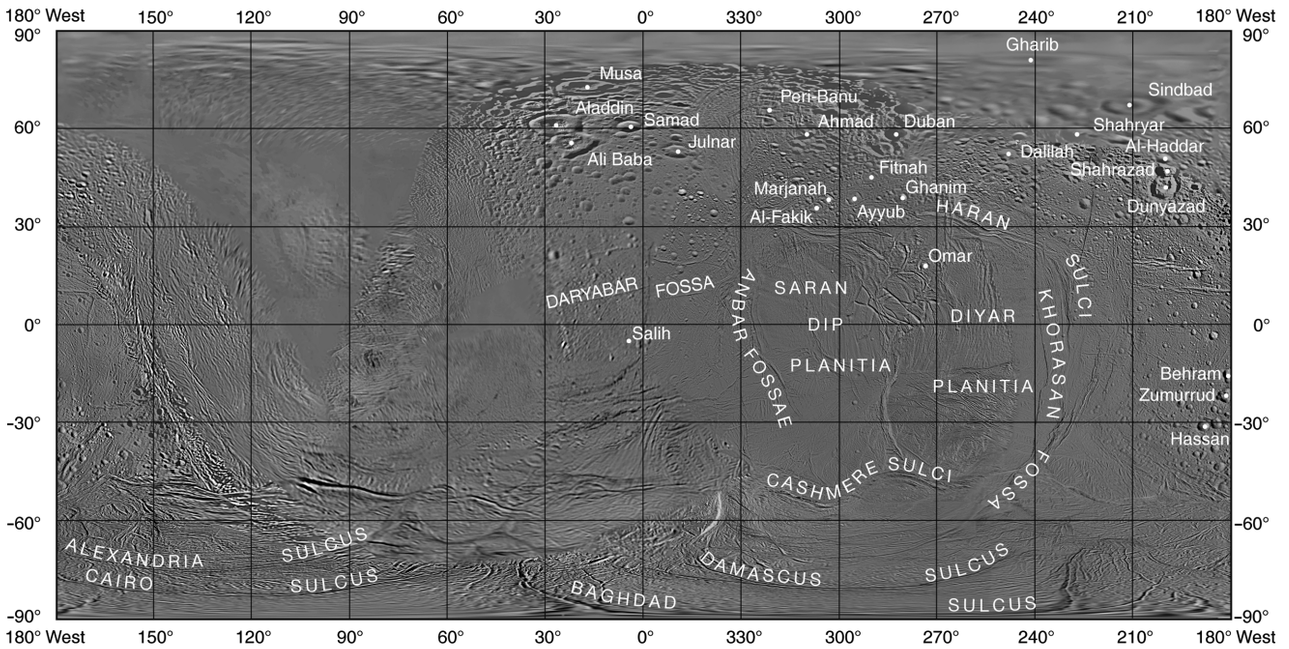

Fig. 24.3 Global mosaic of Enceladus. The map exhibits a map scale of 0.11 km/pixel

– 15 quadrangles format for medium sized bodies and high-resolution imaging, used for Enceladus, Tethys, and Dione (Roatsch et al. 2008a, b)

Three map sheets of Enceladus, Tethys, and Dione are shown in Figures 24.12–24.14 as examples of the atlases. We did not generate a high-resolution atlas of Rhea so far since a new Cassini basemap has yet to be produced. Resolution and scale of the atlases are given in Table 24.6.

The Enceladus atlas was generated using a basemap, which was calculated using the flyby data from 2004 to 2005, no longitude shift as described in Section 24.3.2 was applied for

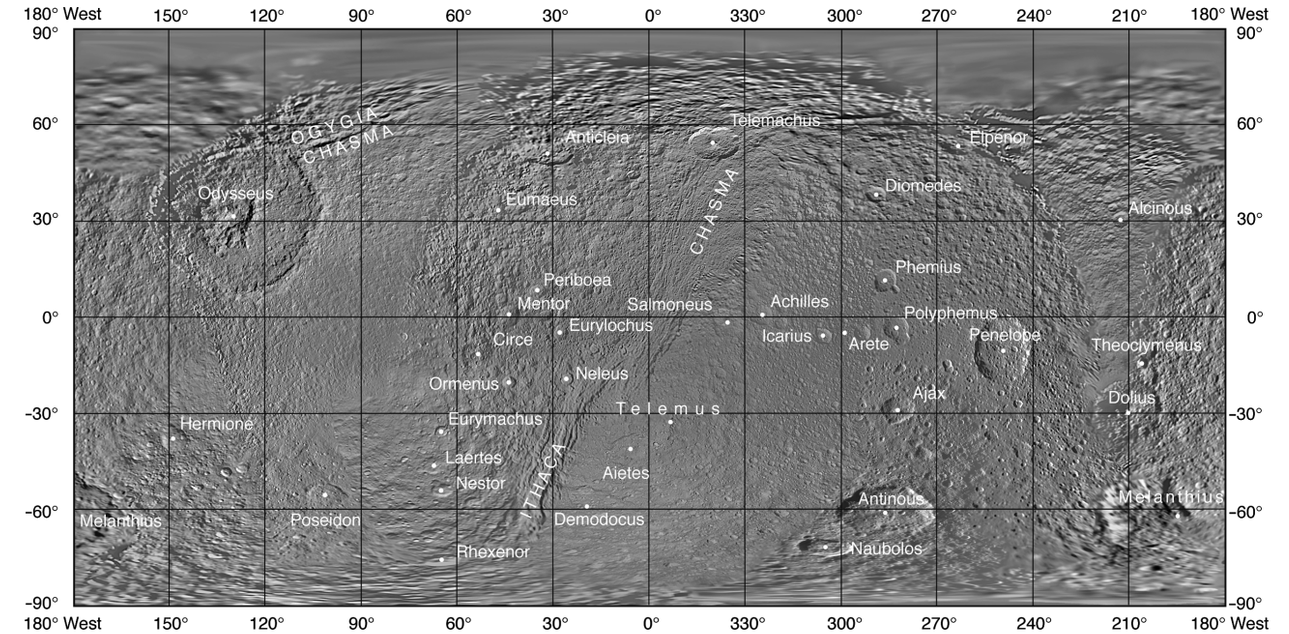

Fig. 24.4 Global mosaic of Tethys. The map exhibits a map scale of 0.29 km/pixel

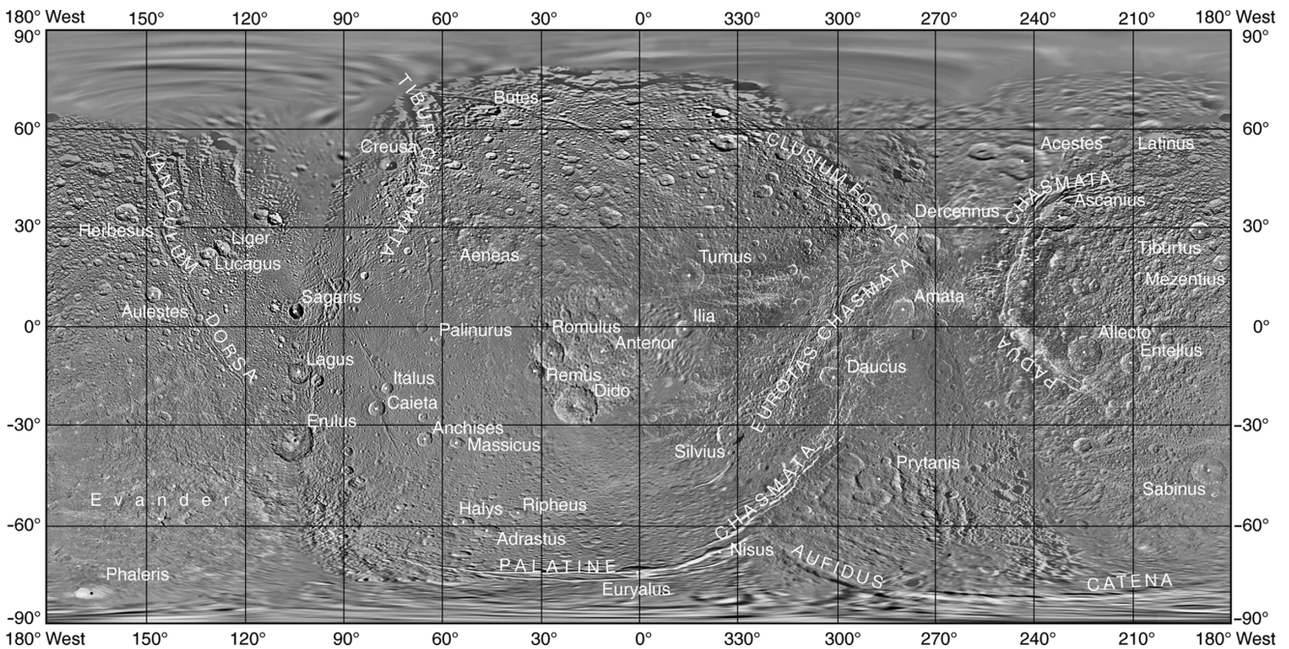

Fig. 24.5 Global mosaic of Dione. The map exhibits a map scale of 0.15 km/pixel

this basemap and the current atlas (Roatsch et al. 2008a). Crater Salih, which determines the longitude system on Enceladus, was imaged with high resolution during the flyby in March 2008, which allowed us to determine the necessary longitude shift also for Enceladus. The basemap shown in Fig. 24.3 and the south pole map sheet shown in Fig. 24.12 were shifted accordingly. A new version of the complete atlas is planned for 2010 after the end of the Cassini extended mission.

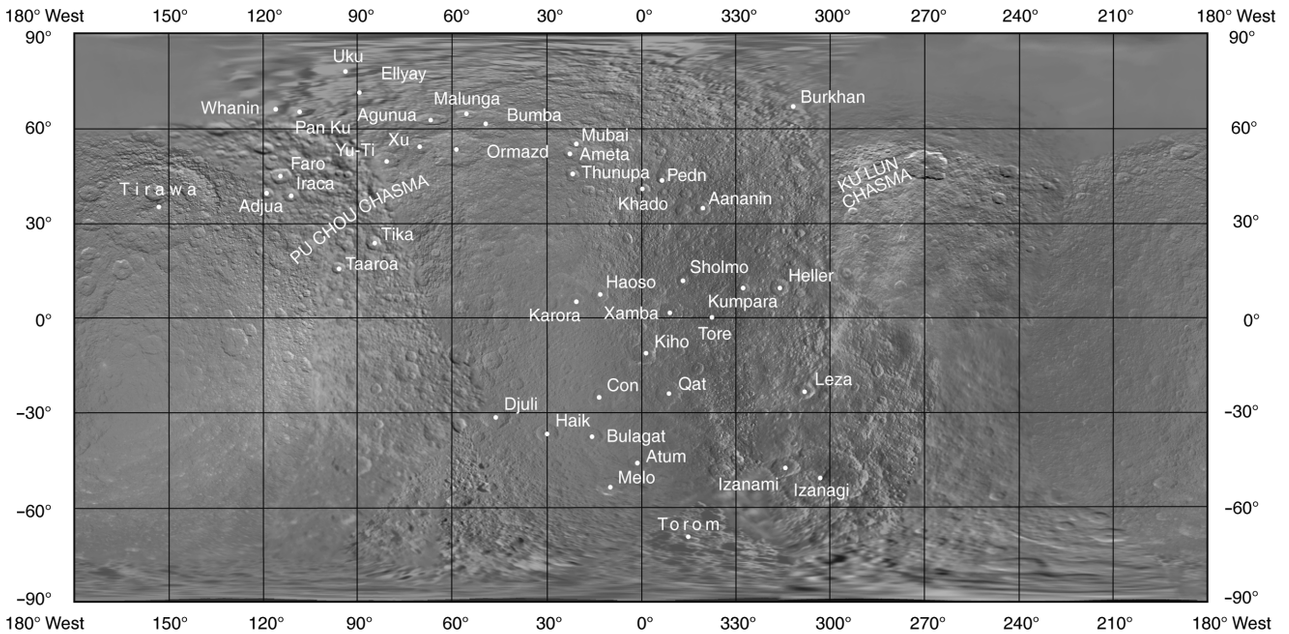

Fig. 24.6 Global mosaic of Rhea (Voyager nomenclature only). The map exhibits a map scale of 0.67 km/pixel

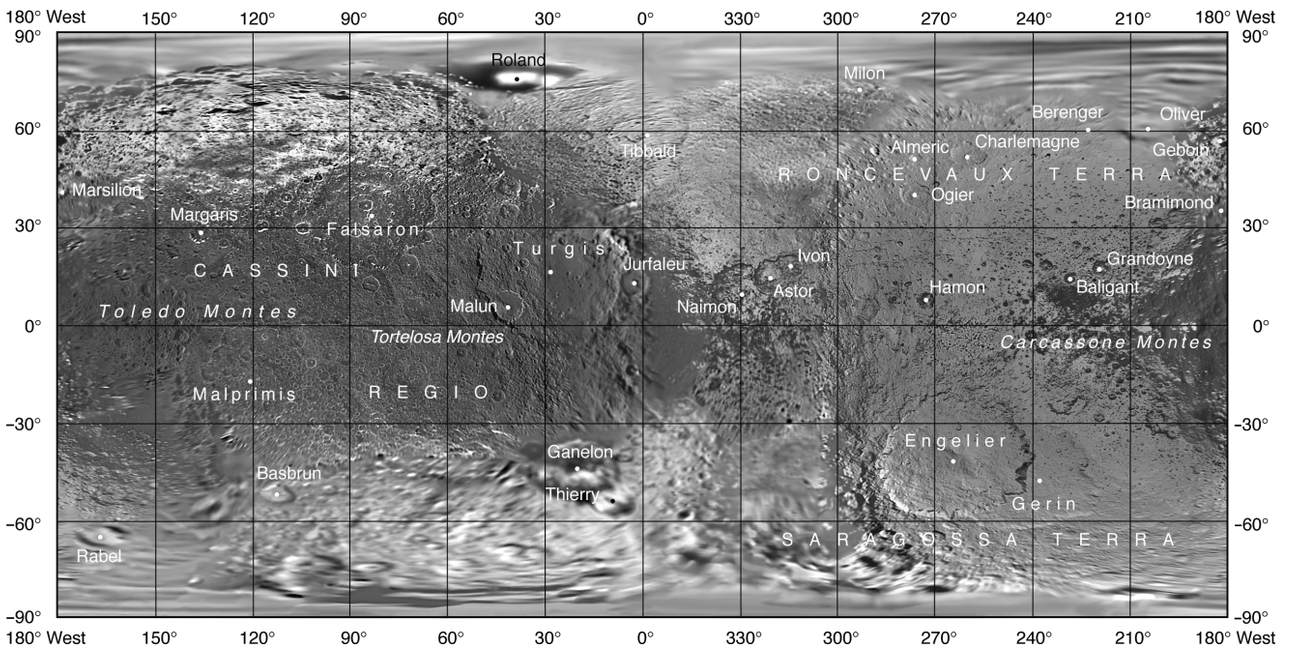

Fig. 24.7 Global mosaic of Iapetus. The map exhibits a map scale of 0.8 km/pixel

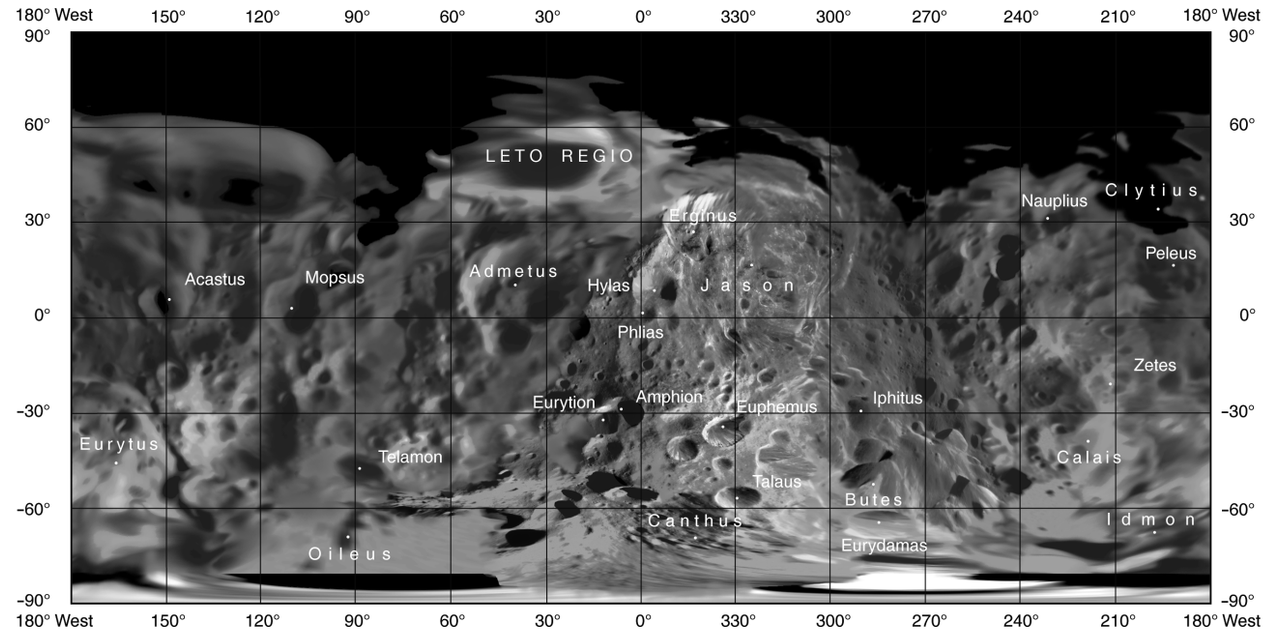

Fig. 24.8 Global mosaic of Phoebe. The map exhibits a map scale of 0.23 km/pixel

Table 24.5 Epics used for feature names on the Saturnian satellites

Satellite	Epic	References
Mimas	Le Morte d' Arthur	Baines (1962)
Enceladus	The Thousand Nights and a Night	Burton (1900)
Tethys	The Odyssey of Homer	Bates (1929)
Dione	The Aeneid of Virgil	Mandelbaum (1972)
Rhea	Names are characters and places from creation myths selected from various cultures around the world; Asian names were emphasized.	
Iapetus	The Song of Roland	Sayers (1967)
Phoebe	The Argonautica	Mozley (1934)

24.5 Compositional Maps Derived from Cassini-VIMS Data

24.5.1 Data Processing

The Visual Infrared Mapping Spectrometer VIMS onboard the CASSINI spacecraft obtained new spectral data of the icy Saturnian satellites after its arrival at Saturn in June 2004. VIMS operates in a spectral range from 0.35 to 5.2 μm, generating image cubes in which each pixel represents a spectrum consisting of 352 contiguous wavebands (Brown et al. 2004). As an imaging spectrometer VIMS combines the characteristics of both a spectrometer and an imaging instrument. This makes it possible to analyze the spectrum of each pixel separately and to map the spectral characteristics spatially, which is important to study the relationships between spectral information and geological and geomorphologic surface features.

VIMS maps presented here show the global coverage achieved by VIMS during Cassini's nominal mission. The re-projection and mosaicking procedures that were applied to the VIMS data are described in detail by Jaumann et al. (2006) and include the following steps:

1. The spatial analysis of the spectral data requires the determination of the exact geographic position of each pixel on the specific surface and that all 352 spectral elements of each pixel show the same region of the target. Therefore the position of each pixel was geometrically corrected and the spectral data converted into map projected image cubes. A nearest-neighbor algorithm was used in order to not modify the original spectra and the map resolution of the map-projected VIMS cubes oversamples the original pixel ground resolution at least by a factor of two to avoid any loss of spatial (and spectral) information. In order to guarantee the accuracy of the VIMS maps and mosaics their quality have been checked by comparison with maps of Voyager and Cassini ISS imaging data (Roatsch et al. 2006). Usually the accuracy of maps based on lower spatial resolution VIMS data is within the limit of one VIMS pixel. If the inaccuracy exceeds one pixel, an additional registration of the VIMS data to ISS basemaps has been applied.

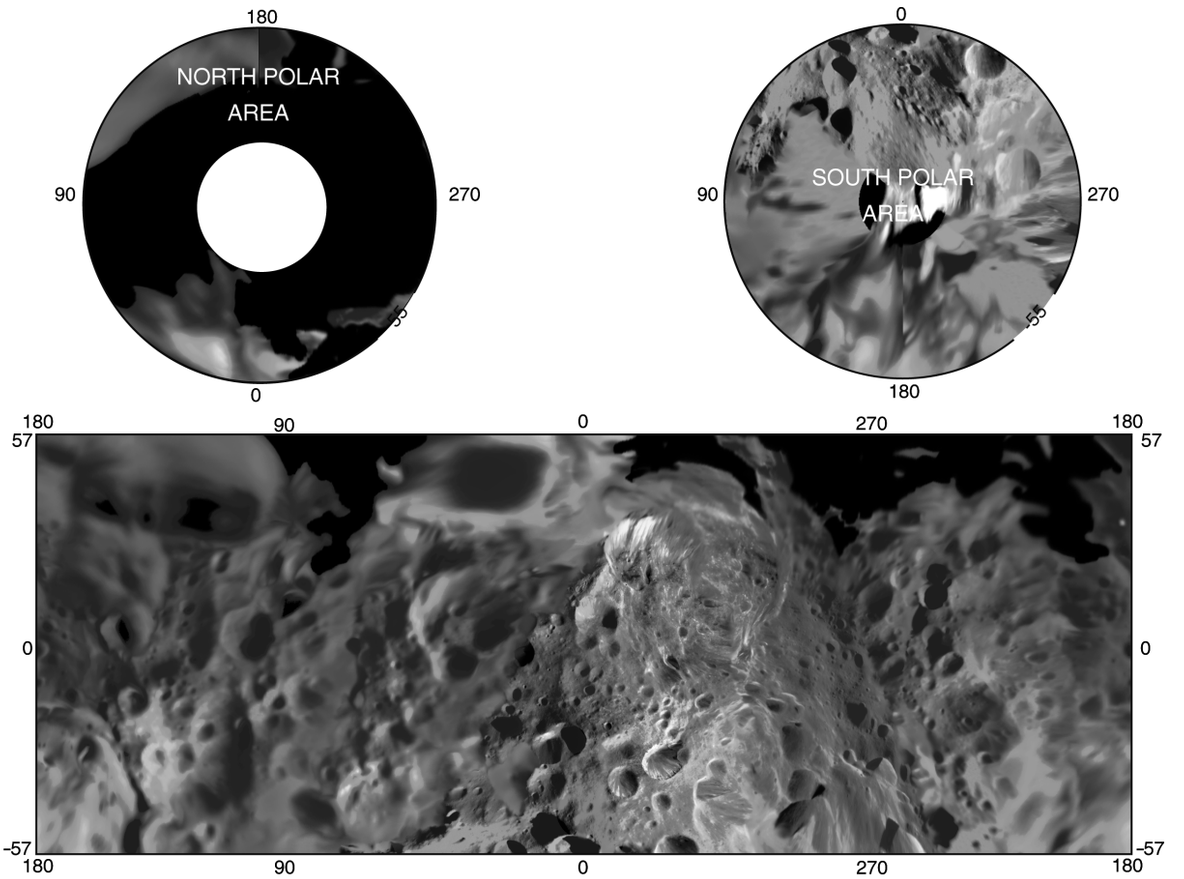

Fig. 24.9 Synoptic format for making planetwide maps on a single sheet. Filled with Phoebe data

2. In order to reduce the influences of the viewing geometry (i.e. incidence, emission and phase angle), that greatly varies between the VIMS observations acquired during Cassini's numerous flybys, in the resulting global VIMS maps, key spectral parameters like the band depths of water ice absorptions were derived according to Clark and Roush (1984) and Clark et al. (2003) for each single map-projected VIMS cube. These band depths are known to indicate changes in the abundance of main surface compounds i.e. water ice and visually dark non-ice materials in the surface material of icy satellites (Clark et al. 2008; Stephan et al. 2009b) but also the sizes and/or crystallinity of water ice particles (Jaumann et al. 2008).
3. Finally, multiple VIMS band depth maps were combined into global VIMS mosaics. Individual projected VIMS maps that were incorporated into a VIMS mosaic were selected according to the following criteria: 1. pixel ground resolution, 2. signal-to-noise ratio, and 3. illumination conditions. Only VIMS cubes with an original pixel ground resolution of at least 150 km/pixel were included into the final mosaics. The individual maps were sorted by pixel ground resolution and signal-to-noise ratio, and the image cube with the highest resolution is located on top of the mosaic. A map resolution of 1 km/pixel was chosen for the final mosaics defined by the VIMS cube with the highest spatial resolution of the specific set. No limb observations were used in the mosaicking process. All resulting VIMS maps were overlaid onto Cassini basemaps in order to relate spectral properties to the surface geology and morphology seen in ISS data.

Progressed mapping by the VIMS instrument during Cassini's nominal mission has been done for the Saturnian satellites Dione, Rhea and Enceladus and will be presented in detail below.

24.5.2 VIMS Composition Map of Dione

Dione was observed during two targeted flybys (16, 50) in October 2005 and September 2007 and also during the

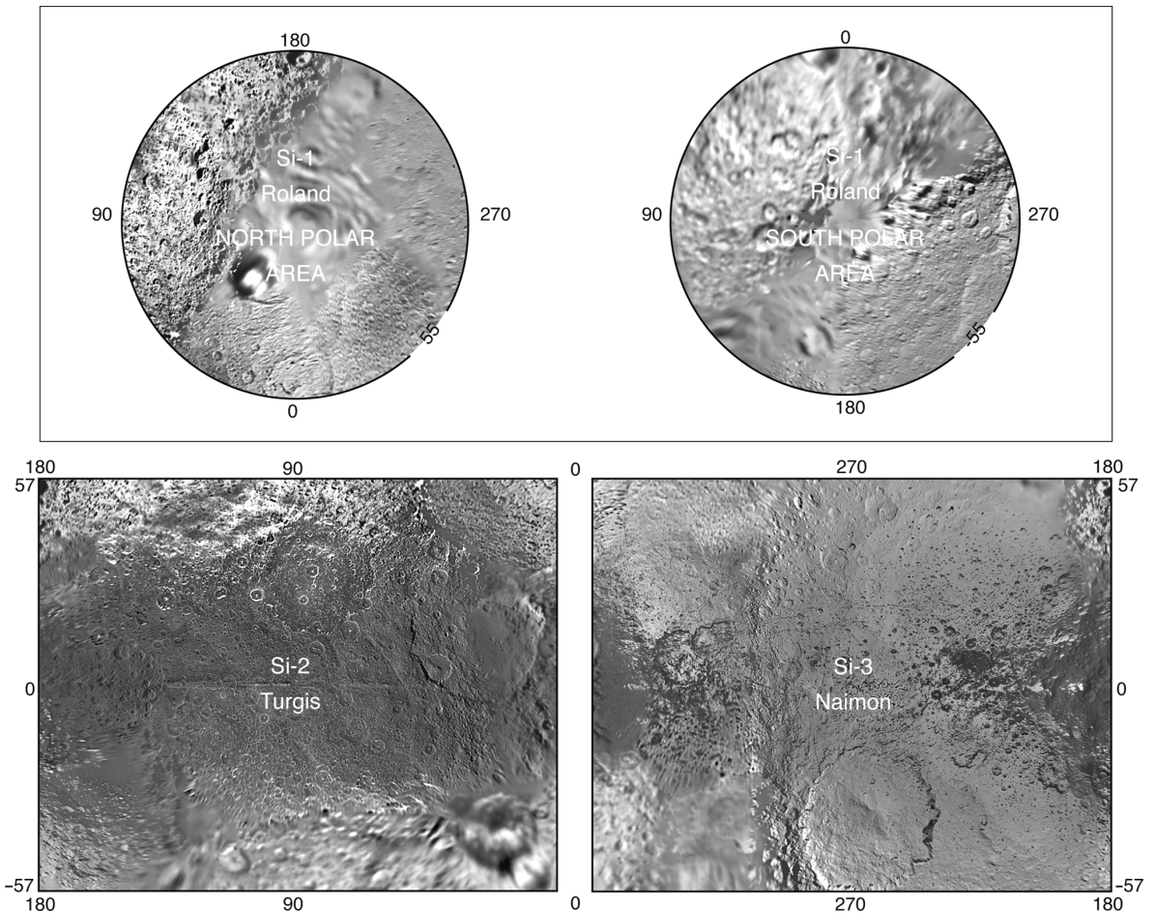

Fig. 24.10 Subdivision of the synoptic format for making planetwide maps on three sheets. Filled with Iapetus data

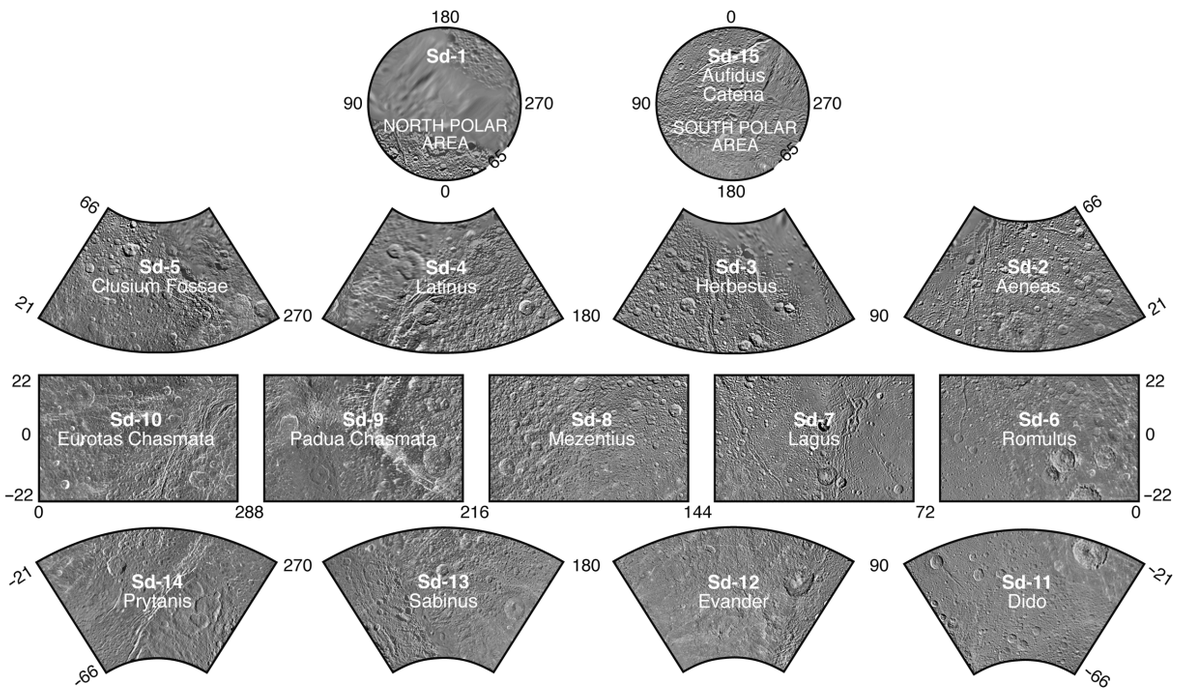

Fig. 24.11 The schema for medium sized bodies and high-resolution imaging with 15 quadrangles. Filled with Dione data

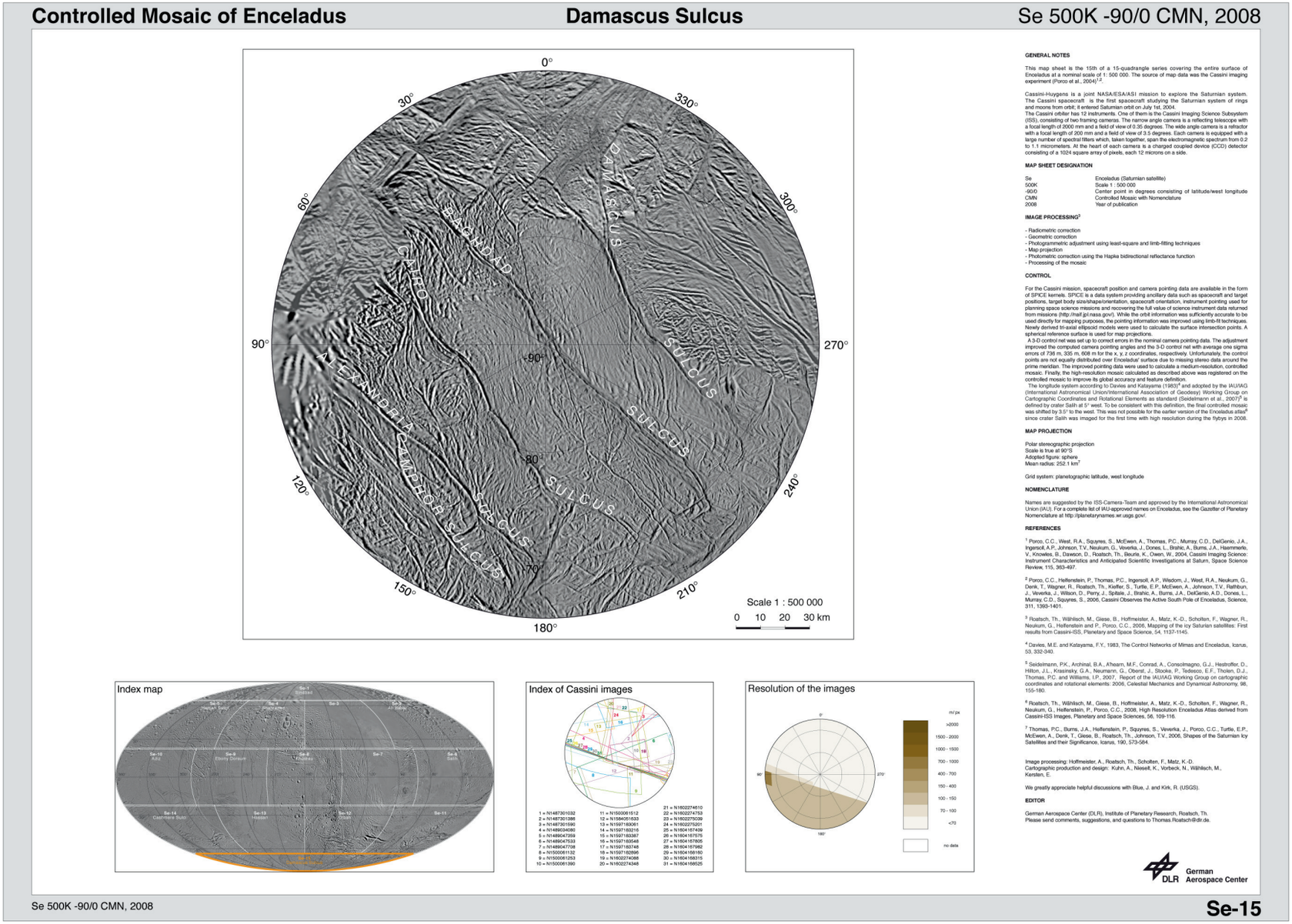

Fig. 24.12 Enceladus map sheet 15: Damascus Sulcus

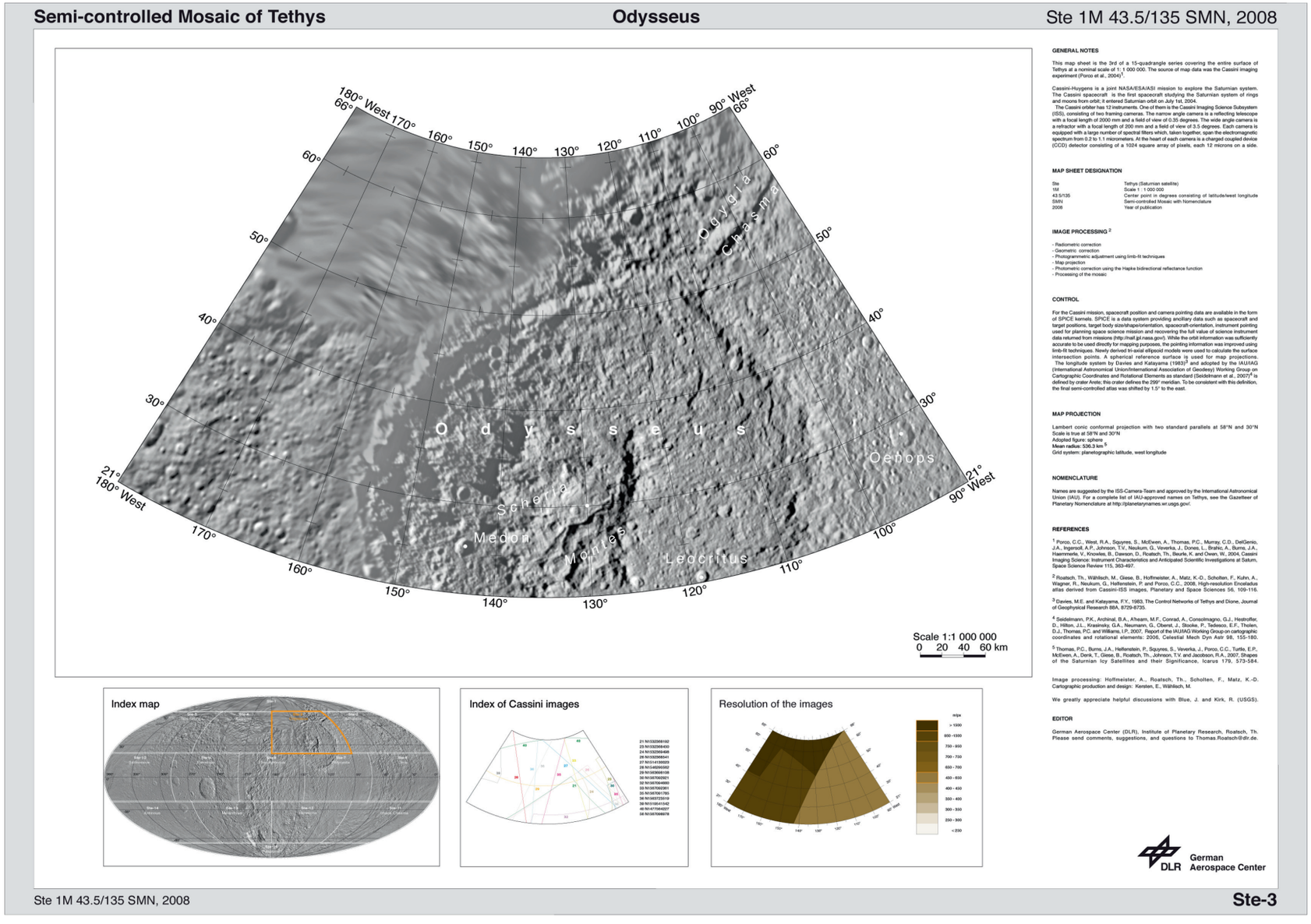

Fig. 24.13 Tethys map sheet 3: Odysseus

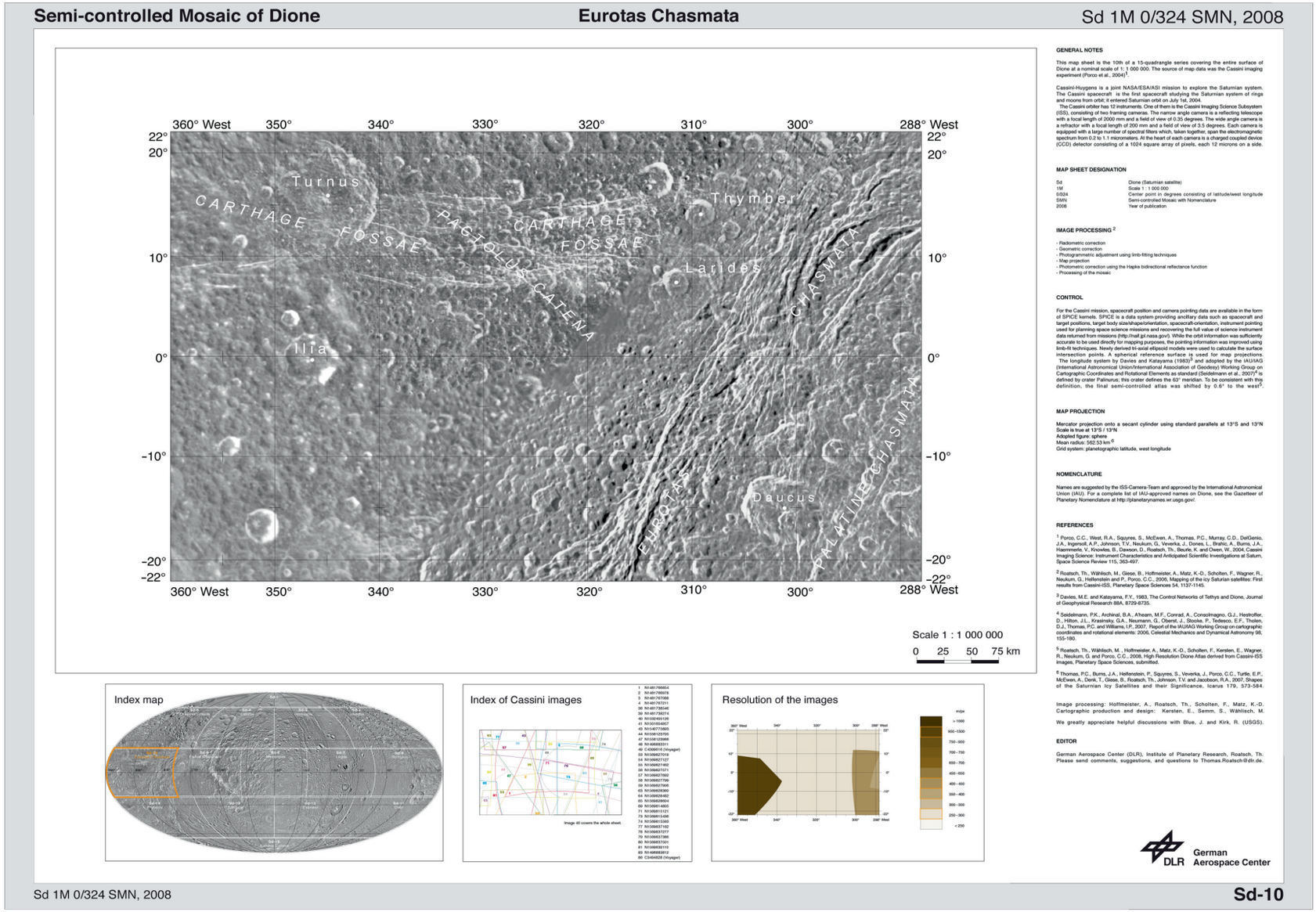

Fig. 24.14 Dione map sheet 10: Eurotas Chasmata

Table 24.6 Resolution and scale of the mosaics and atlases

Satellite	Mean radius used for the map projection (km)	Resolution of the map digmap (pixel/°)	Map scale of the atlas
Mimas	198.8	8	1:1,500,000
Enceladus	252.1	40	1:500,000
Tethys	536.3	32	1:1,000,000
Dione	562.53	64	1:1,000,000
Rhea	764.0	20	–
Iapetus	736.0	16	1:3,000,000
Phoebe	106.8	8	1:1,000,000

non-targeted flybys B, 9, 26, 27 and 43 with sufficient pixel ground resolution of better than 150 km/pixel (Table 24.7). This resulted into a complete VIMS coverage of this satellite. Especially the trailing hemisphere is best covered by high-resolution observations. Best pixel ground resolutions (<5 km/pixel) were achieved during the observation sequence DIONE205 in orbit 16 with the closest approach to Dione's surface of 498 km (Stephan et al. 2009b). During orbit B and 50 the satellite was still observed with 10 to 40 km/pixel. However, during orbits 9, 26, and 27 pixel ground resolutions only occasionally are better than 40 km/pixel. Nevertheless the acquired VIMS data provide the context information to the highly resolved VIMS data. This is also the case for Dione's leading hemisphere which was observed mainly during orbit 43 (Table 24.7).

Figure 24.15 shows a global VIMS map of Dione that illustrates the color coded spatial variations of the water ice absorption depth at 1.5 μm. Especially, the increasing amount of the dark non-ice material in the surface material of Dione, that is concentrated on its trailing hemisphere, is known to reduce the depth of this water ice absorption significantly. For scientific discussion the reader is referred to the work of Clark et al. (2008) and Stephan et al. (2009b).

24.5.3 VIMS Composition Map of Rhea

Since July 2004 numerous flybys were performed at Saturn's satellite Rhea (Table 24.8). VIMS data acquired during 11 flybys (up to Cassini's 54th orbit in December 2007) exhibiting pixel ground resolutions of at least 150 km/pixel were incorporated into the global VIMS map in Fig. 24.16 (Stephan et al. 2009a). Despite of the polar regions, Rhea's surface has been observed by VIMS almost completely. However, most observations exhibit relatively low pixel ground resolutions of less than 40 km/pixel. Only VIMS observations of Rhea's anti-Saturnian hemisphere acquired during one non-targeted flyby (Cassini orbit 49 on Aug. 30, 2007) reach pixel ground resolutions of about 1 km/pixel.

Like presented for Dione the resulting map shows the variations in band depth of the water ice absorption at 1.5 μm dominated by the varying amount of water ice and visually dark rocky material (Stephan et al. 2009a).

24.5.4 VIMS Composition Map of Enceladus

The Saturnian satellite Enceladus was observed during the targeted flybys 3, 4, 11 and 61 in March and July 2005 and in March 2008, respectively, as well as the quasi-targeted flyby 3 in February 2005 with sufficient pixel ground resolution and signal-to-noise ratio. Best pixel ground resolutions achieved during orbit 11 reached 1 km/pixel (Table 24.9) and covers especially the trailing hemisphere between 180° and 360° W including Enceladus' South Polar Region. In contrast, the coverage of the leading hemisphere from 0° and 180° W is still very rare and remains to be a completed during Cassini's extended (equinox) mission through the Saturnian system.

Figure 24.17 shows the global VIMS map produced for Enceladus. Like shown for Dione and Rhea this color coded map also illustrates the variations in depth of the water ice absorption at 1.5 μm. However, the surface material on Enceladus consists of pure water ice (Brown et al. 2006; Jaumann et al. 2008). Therefore, variations in band depth are here indicative to the varying sizes of the water ice particles as described in the work of Jaumann et al. (2008). Figure 24.18 shows the particle size map separately for the South Polar Region of Enceladus including the so called 'tiger stripes' (Porco et al. 2006).

24.6 Future Work

The Cassini spacecraft will continue its imaging campaign through the Saturnian system through at least 2010. The upcoming flybys will help to replace the low-resolution parts of the mosaics and atlases with higher resolution image data derived from ISS images. This will be also an important step for the VIMS coverage of Saturn's satellites in addition to the completion of VIMS coverage of Enceladus and the remaining mid-sized satellites Iapetus, Tethys and Mimas that were not or only preliminary mapped so far. The northern part of the Saturnian satellites will be illuminated during the extended (equinox) mission providing a unique opportunity to obtain high-resolution Cassini coverage of high northern latitudes.

Table 24.7 VIMS observations of Dione combined into the global map in Fig. 24.15

Cassini orbit	Observation time	VIMS Observations sequences	Number of cubes	Geographic location	Average pixel ground resolution of the input cubes (km/pixel)
00B	Dec. 2004	REGMAP001	3	47°N–52°S/276–350°W	25–17.4
		GLOCOL001	2	60°N–55°S/140–280°W	∼38
009	June 2005	DIONE001	13	35°N–70°S/164–275°W	79.3–40.8
016	Oct. 2005	DIONE205	32	60°N–85°S/96–260°W	44.5–2.9
026	July 2006	GLOCOL001	4	60°N–60°S/245–340°W	63.8–64.8
027	Aug. 2006	REGEODB001	30	67°N–37°S/240°–320°W	66.5–97.4
		REGEODC001	24	60°N–17°S/220°–330°W	102–150
043	Apr. 2007	REGMAPB001	5	40°N–90°S/100–360°W	29.5–60.6
050	Sep. 2007	DIONE001	4	60°N–75°S/350–250°W	27.2–23.3
		DIONE002	6	70°N–60°S/276–67°W	13.3–29.1
		REGMAPE001	17	60°N–75°S/250–320°W	16.2–32.6
		REGMAPF001	31	76°N–70°S/270–50°W	10.0–21.5
		REGMAPG001	13	67°N–70°S/85–310°W	24.3–87.4

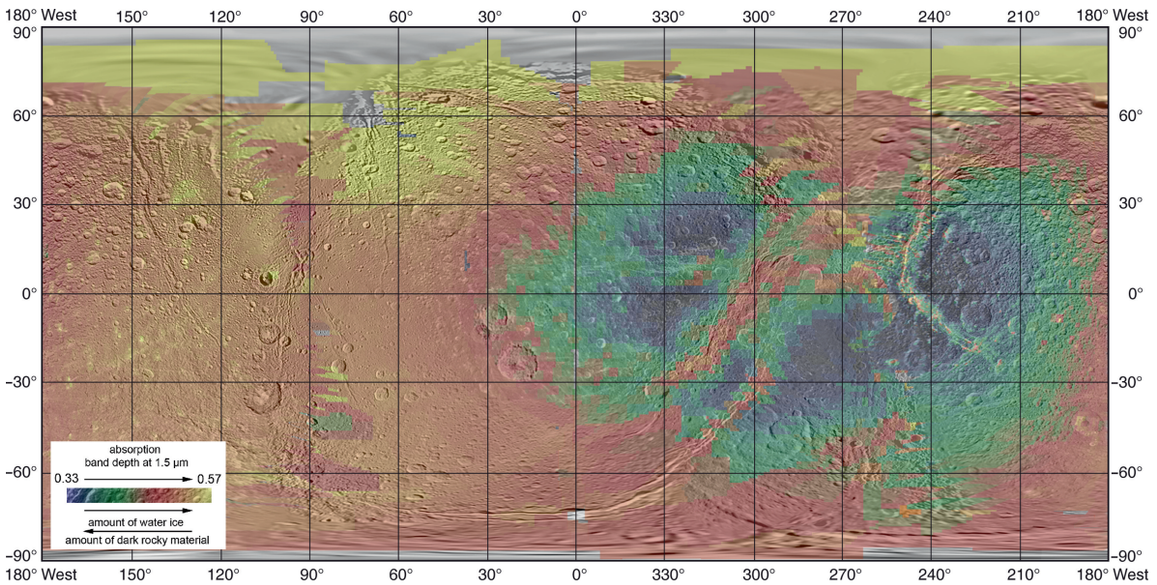

Fig. 24.15 Global VIMS composition map of Dione based on VIMS observations summarized in Table 24.7 in a simple cylindrical map projection overlaid onto the corresponding ISS basemap. The map exhibits a map scale of 1 km/pixel (Stephan et al. 2009b)

Table 24.8 VIMS observations of Rhea combined into the global map in Fig. 24.16

Cassini orbit	Observation time	VIMS Observations sequences	Number of cubes	Geographic location	Average pixel ground resolution of the input cubes (km/pixel)
00C	Jan. 2005	RHEA003	4	38°N–87°S/178–334°W	38.4–36.3
		RHEA004	4	44°N–80°S/346–174°W	40.8–39.6
		RHEA005	3	42°N–76°S/48–186°W	43.0–41.7
		RHEA006	4	55°N–77°S/25–174°W	46.5–45.2
		RHEA007	4	52°N–76°S/44–182°W	54.3–50.7
		RHEA102	2	88°N–68°S/250–36°W	120.3–119.7
003	Feb. 2005	RHEA101	5	64°N–90°S/10–170°W	84.8–81.0
005	Mar. 2005	RHEA001	12	60°N–75°S/15–160°W	66.3–33.1
006	Apr. 2005	RHEA001	8	60°N–88°S/10–165°W	59.3–57.3

(continued)

Table 24.8 (continued)

Cassini orbit	Observation time	VIMS Observations sequences	Number of cubes	Geographic location	Average pixel ground resolution of the input cubes (km/pixel)
011	July 2005	RHEA001	2	20°N–90°S/0°–360°W	60.5–60.0
		RHEA002	8	10°N–88°S/0°–360°W	56.7–50.5
		RHEA003	6	30°N–90°S/330°–270°W	82.4–79.5
		RHEA004	4	6°S–90°S/0–360°W	43.6–43.1
012	Aug. 2005	RHEA001	16	26°N–90°S/0–360°W	64.6–61.6
		RHEA003	6	34°N–90°S/0–360°W	52.7–52.0
		RHEA004	3	40°N–90°S/100–360°W	55.7–55.5
018	Nov. 2005	RHEA002	8	88°N–64°S/90°–248°W	48.0–29.1
		RHEA111	16	60°N–75°S/350–250°W	42.5–32.9
		RHEA112	14	40°N–40°S/110°–180°W	19.7–16.2
019	Dec. 2005	RHEA101	14	70°N–64°S/148°–270°W	81.5–74.5
020	Jan. 2006	RHEA002	6	74°N–54°S/230°–15°W	57.2–54.7
022	Mar. 2006	RHEA002	4	63°N–70°S/268°–28°W	34.9–34.45
		RHEA003	9	32°N–45°S/168–10°W	33.8–28.7
		RHEA004	3	62°N–72°S/285–46°W	26.8–26.4
		RHEA006	3	58°N–75°S/310–48°W	23.1–22.6
049	Aug. 2007	RHEA001	6	68°N–66°S/350°–80°W	39.5–32.2
		RHEA010	34	58°N–72°S/96–340°W	6.28–1.32
		RHEA011	19	72°N–48°N/−90°–240°W	8.48–6.87

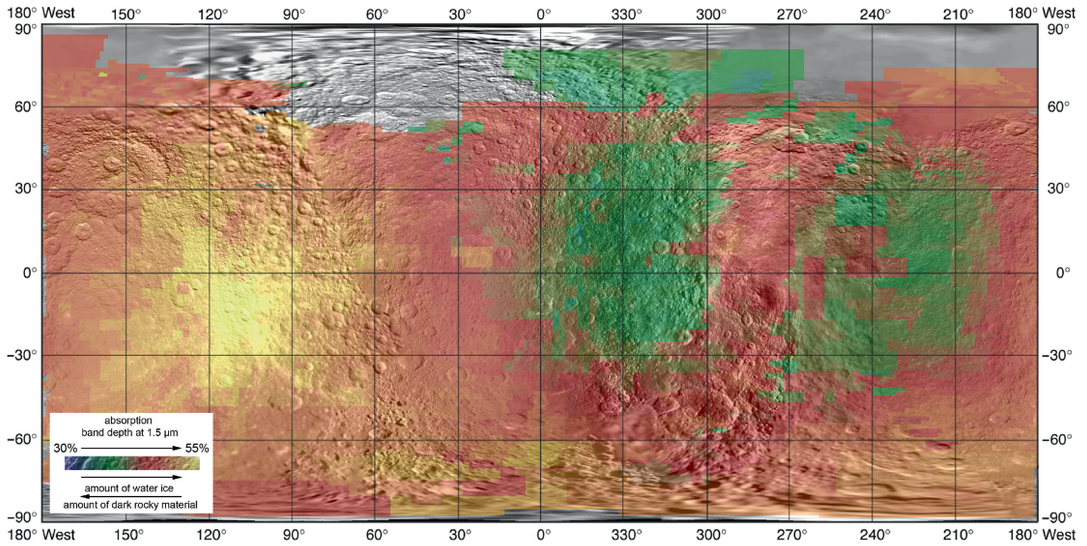

Fig. 24.16 Global VIMS composition map of Rhea based on VIMS observations summarized in Table 24.8 in a simple cylindrical map projection pixel overlaid onto the corresponding ISS basemap. The map exhibits a map scale of 1 km/pixel (Stephan et al. 2009a)

Table 24.9 VIMS observations of Enceladus that were combined into the global map in Fig. 24.17

Cassini orbit	Observation time	VIMS Observations sequences	Number of cubes	Geographic location	Average pixel ground resolution of the input cubes (km/pixel)
003		ENCELADUS007	13	68°N–77°S/2°–229°W	7.7–2.6
004	Mar 2005	ENCELADUS019	7	70°N–30°S/160–260°W	10.2–13.2
011	July 2005	ENCELADUS108	4	30°N–90°S/160–280°W	30.3–13.2
		ENCELADUS110	5		18.2–1.0
		ENCELADUS111	14		6.85–3.6
061		ENCELADUS002	14	90°–8.5°N/250°–60°W	22.5–18.5
		ENCELADUS005	2		25.8–25.4
		ENCELADUS007	3		8.2–6.8

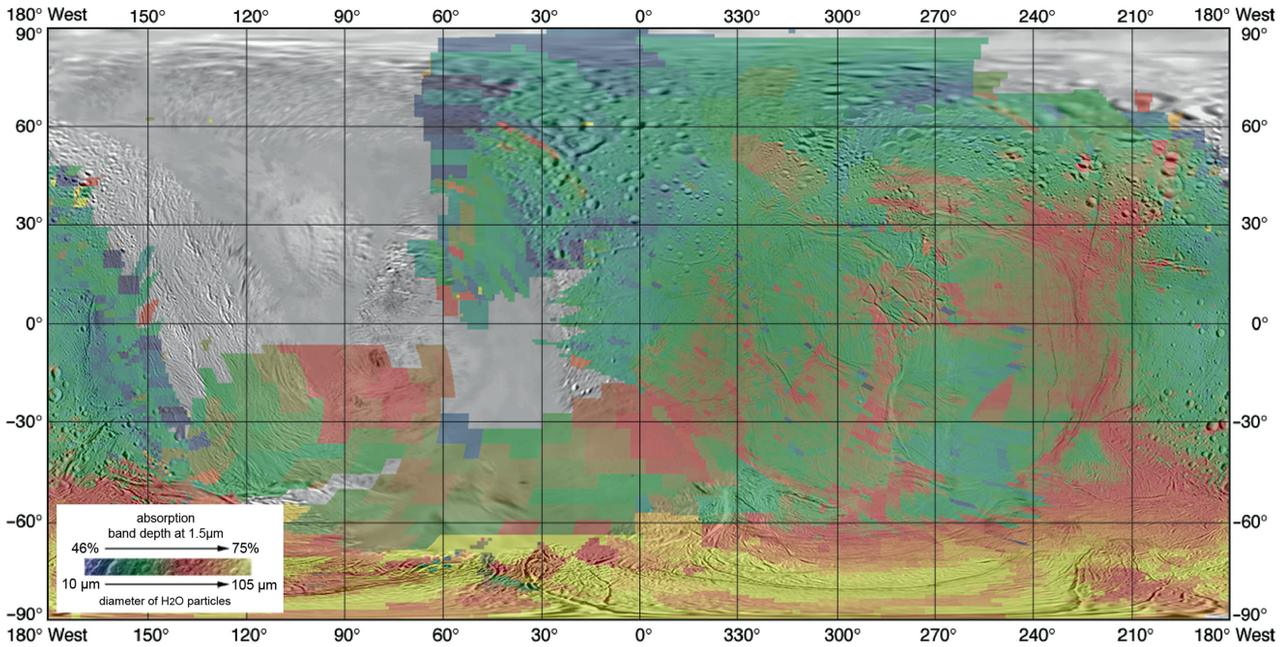

Fig. 24.17 Global VIMS composition map of Enceladus based on VIMS observations summarized in Table 24.9 in a simple cylindrical map projection pixel overlaid onto the corresponding ISS basemap. The map exhibits a map scale of 1 km/pixel (after Jaumann et al. 2008)

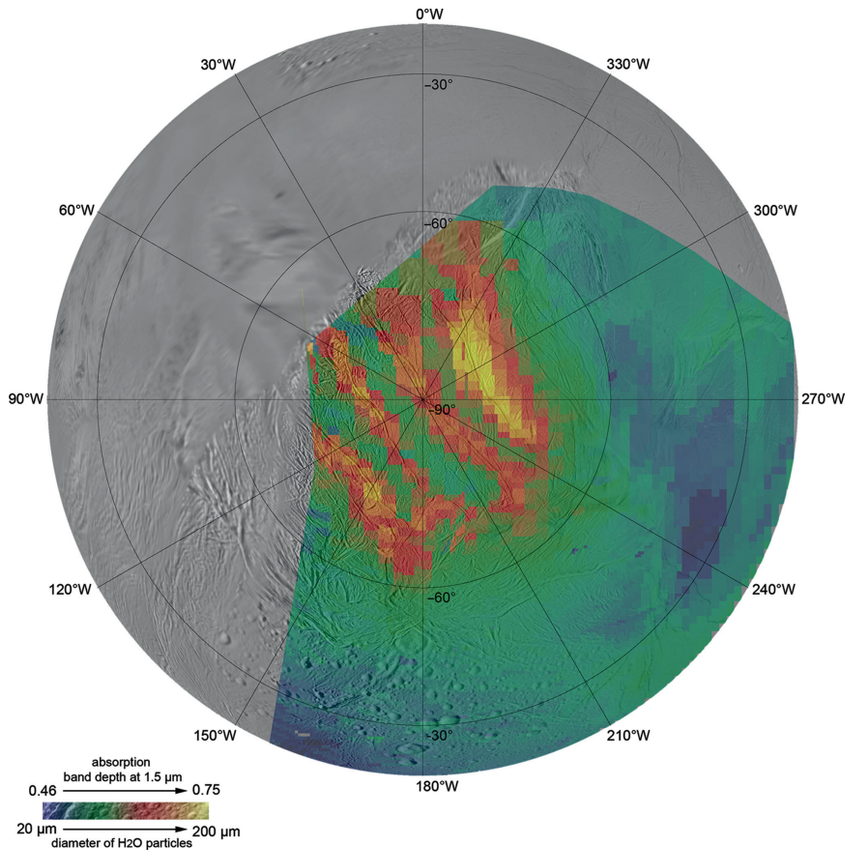

Fig. 24.18 VIMS mosaic of the South Polar Region illustrating the particle size variations derived by VIMS measurements using data of observation sequence ENCELADUS111 (Table 24.9) of orbit 11 overlaid onto the corresponding ISS map (after Jaumann et al. 2008)

Acknowledgements The authors gratefully acknowledge the work for the software development, image processing and the generation of the atlases of M. Wählisch, A. Hoffmeister, E. Kersten, K.-D. Matz, F. Scholten, R. Wagner, and B. Giese (DLR). They also acknowledge the image planning and camera operation work of their colleagues from the Cassini imaging team especially the operations team at the Cassini Imaging Central Laboratory for Operations (CICLOPS). Furthermore, they acknowledge helpful discussions with J. Blue and R. Kirk (USGS) about the proposed feature nomenclature and for reviewing the atlases. Finally, the authors acknowledge the planning and operation work of their colleagues from the Cassini VIMS team.

References

Baines, K., 1962: *Malor's Le Morte d'Arthur*. Mentor, New York.

Bates, H., 1929: *The Odyssey of Homer*. Harper and Brothers, New York.

Batson, R., 1984: Voyager 1 and 2 Atlas of Six Saturnian Satellites. Scientific and Technical Information Branch, National Aeronautics and Space Administration, Washington, D.C., http://history.nasa.gov/SP-474/sp474.htmp.

Brown, R.H., Baines, K.H., Bellucci, G., Bibring, J.-P., Burratti, B.J., Bussoletti, E., Capaccioni, F., Cerroni, P., Clark, R.N., Coradini, A., Cruikshank, D.P., Drossart, P., Formisano, V., Jaumann, R., Langevin, Y., Matson, D.L., McCord, T.B., Miller, E., Nelson, R.M., Nicholson, P.D., Sicardy, B., and Sotin, C., 2004: The Cassini Visual and Infrared Mapping Spectrometer Investigation. Space Science Reviews 115, 111–168.

Brown, R.H., Clark, R.N., Buratti, B.J., Cruikshank, D.P., Barens, J.W., Mastrapa, R.M.E., Bauer, J., Newman, S., Momary, T., Baines, K.H., Bellucci, G., Capaccioni, P., Cerroni, P., Combes, M., Coradini, A., Drossart, P., Formisano, V., Jaumann, R., Langevin, Y., Matson, D.L., McCord, T.B., Nelson, R.M., Nicholson, P.D., Sicardy, B., and Sotin, C., 2006: Composition and physical properties of Enceladus' surface. Science 311, 1425–1428.

Burton, R., 1900: Alf Laylah Wa Laylah, *The Book of the Thousand Nights and a Night*. Larsen-Harper, Colorado Press, Denver, CO.

Castillo-Rogez, J.C., Matson, D.L., Sotin, C., Johnson, T.V., Lunine, J.I., Thomas, P.C., 2007: Iapetus' geophysics: Rotation rate, shape, and equatorial ridge. Icarus 190, 179–202.

Chandrasekhar, S., 1969: *Ellipsoidal Figures of Equilibrium*, Yale University Press, New Haven.

Charnoz, S., Brahic, A., Thomas, P.C., and Porco, C.C., 2007: The equatorial ridges of Pan and Atlas: Terminal accretionary ornaments?. Science 318, 1622.

Clark, R.N. and Roush, T.L., 1984: Reflectance spectroscopy: Quantitative analysis techniques for remote sensing applications. J. Geophys. Res. 89, 6329–6340.

Clark, R.N., Swayze, G.A., Livo, K.E., Kokaly, R.F., Sutley, S.J., Dalton, J.B., McDougal, R.R., and Gent, C.A., 2003: Imaging spectroscopy: Earth and planetary remote sensing with the USGS Tetracorder and expert systems. J. Geophys. Res. 108(E12), 5131, doi:10.1029/2002JE001847.

Clark, R., Brown, R.H., Jaumann, R., Cruikshank, D.P., Buratti, B., Baines, K.H., Nelson, R.N., Nicholson P.D., Moore, J.M., Curchin, J., Hoefen, T., and Stephan, K., 2008: Compositional mapping of Saturn's Satellite Dione with Cassini VIMS and implications of dark material in the Saturnian system. Icarus 1933, 72–386.

Davies, M. E. and Katayama, F. Y., 1983a: The control networks of Mimas and Enceladus. Icarus 53, 332–340.

Davies, M.E. and Katayama, F.Y., 1983b: The control networks of Tethys and Dione. Journal of Geophysical Research 88A, 8729–8735.

Davies, M. E. and Katayama, F. Y., 1983c: The control network of Rhea. Icarus 56, 603–610.

Davies, M. E. and Katayama, F. Y., 1984: The control network of Iapetus. Icarus 59, 199–204.

Dermott, S. F. and Thomas, P.C., 1988: The shape and internal structure of Mimas. Icarus 73, 25–65.

Greeley, R. and Batson, G., 1990: *Planetary Mapping*. Cambridge University Press.

Jacobson, R.A., Antreasian, P.G., Bordi, J.J., Criddle, K.E., Ionasescu, R., Jones, J.B., Mackenzie, R.A., Pelletier, F.J., Owen, W.M. Jr., Roth, D.C., and Stauch, J.R., 2006: The gravitational field of Saturn and the masses of its major satellites. Astronomical Journal 132, 2520–2526.

Jaumann, R., Stephan, K., Brown, R.H., Buratti, B.J., Clark, R.N., McCord, T.B., Coradini, A., Capaccioni, P., Filacchione, G., Cerroni, P., Baines, K.H., Bellucci, G., Bibring, J.P., Combes, M., Cruikshank, D.P., Drossart, P., Formisano, V., Langevin, Y., Matson, D.L., Nelson, R.M., Nicholson, P.D., Sicardy, B., Sotin, C., Soderblom, L.A., Griffith, C., Matz, K.D., Roatsch, T., Scholten, F., and Porco, C.C., 2006: High-resolution Cassini-VIMS mosaics of Titan and the icy Saturnian satellites. Planetary and Space Science 54, 1146–1155.

Jaumann, R., Stephan, K., Hansen, G.B., Clark, R.N., Buratti, B.J., Brown, R.H., Baines, K.H., Newman, S.F., Bellucci, G., Filacchione, G., Coradini, A., Cruikshank, D.P., Griffith, C.A., Hibbitts, C.A., McCord, T.B., Nelson, R.M., Nicholson, P.D., Sotin, C., and Wagner, R., 2008: Distribution of icy particles across Enceladus' surface as derived from Cassini-VIMS measurements. Icarus 193, 407–419.

Kirk, R.L., Becker, T.L., Rosanova, T., Soderblom, L.A., Davies, M.E., and Colvin, T.R., 1998: Digital maps of the Saturnian satellites – First steps in cartographic support of the Cassini Mission. Jupiter after Galileo, *Saturn before Cassini Conference*, Nantes, France.

Mandelbaum, A., 1972: *The Aeneid of Virgil*. Bantam, New York.

Minton, D.A. 2008: The topographic limits of gravitationally bound, rotating sand piles. Icarus 195, 698–704.

Mozley, J. H., 1934: *The Argonautica, by Valerius Flaccus* (English translation). The Loeb Classical Library, Cambridge, MA.

Porco, C.C. and 19 co-authors, 2004: Cassini imaging science: Instrument characteristics and anticipated scientific investigations at Saturn. Space Science Review 115, 363–497.

Porco, C.C. and 34 co-authors, 2005: Cassini imaging science: Initial results on Phoebe and Iapetus. Science 307, 1237–1242.

Porco, C.C. and 24 co-authors, 2006: Cassini observes the active south pole of Enceladus. Science 311, 1393–1401.

Porco, C.C., Thomas, P.C., Weiss, J.W., and Richardson, D.C., 2007: Saturn's small inner satellites: Clues to their origins. Science 318, 1602.

Roatsch, T., Wählisch M., Scholten, F., Hoffmeister, A., Matz K.-D., Denk, T., Neukum G. Thomas, P., Helfenstein, P., and Porco, C.C., 2006: Mapping of the icy Saturnian satellites: First results from Cassini-ISS. Planetary Space Sciences 54, 1137–1145.

Roatsch, T., Wählisch, M., Giese, B., Hoffmeister, A., Matz, K.-D., Scholten, F., Kuhn, A., Wagner, R., Neukum, G., Helfenstein, P., and, Porco, C.C., 2008a: High-resolution Enceladus atlas derived from Cassini-ISS images. Planetary Space Sciences 56, 109–116.

Roatsch, T., Wählisch, M., Hoffmeister, A., Matz, K.-D., Scholten, F., Kersten, E., Wagner, R., Denk, T., Neukum, G., and Porco, C.C., 2008b: High-resolution Dione atlas derived from Cassini-ISS images. Planetary Space Sciences 56, 1499–1505.

Roatsch, T., Wählisch, M., Hoffmeister, A., Kersten, E., Matz, K.-D., Scholten, F., Wagner, R., Denk, T., Neukum, G., Helfenstein, P., and Porco, C.C., 2009: High-resolution atlases of Mimas, Tethys, and Iapetus derived from Cassini-ISS images. Planetary Space Sciences 57, 83–92.

Sayers, D.L., 1967: *The Song of Roland*. Penguin Books Inc., Baltimore.

Seidelmann, P.K., Archinal, B.A., A'hearn, M.F., Conrad, A., Consolmagno, G.J., Hestroffer, D., Hilton, J.L., Krasinsky, G.A., Neumann, G., Oberst, J., Stooke, P., Tedesco, E.F., Tholen, D.J., Thomas, P.C., and Williams, I.P., 2007: Report of the IAU/IAG Working Group on cartographic coordinates and rotational elements. Celestial Mechanics and Dynamical Astronomy 98, 155–180.

Simonelli, D.P., Thomas, P., Carcich, B.T., and Veverka, J., 1993: The generation and use of numerical shape models for irregular solar-system objects. Icarus 103, 49–61.

Stephan, K., Jaumann, R., Wagner, R., Clark, R., Cruikshank, D.P., Hibbitts, C.A., Roatsch, T., Brown, R.H., Buratti, B.J., Filiacchione, G., Hansen, G.B., McCord, T.B., Baines, K.H., and Nicholson, P.D., 2009a: VIMS coverage of Saturn's icy satellite Rhea. LPSC, 1377.

Stephan, K. Jaumann, R., Wagner, R., Clark, R.N., Cruikshank, D.P., Hibbitts, C.A., Roatsch, T., Hoffmann, H., Brown, R.H., Filiacchione, G., Buratti, B.J., Hansen, G.B., McCord, T.B., Nicholson, P.D., and Baines, K.H., 2009b: Dione's spectral and geological properties, submitted to Icarus.

Thomas, P.C., Davies, M.E., Colvin, T.R., Oberst, J., Schuster, P., Neukum, G., Carr, M.H., McEwen, A., Schubert, G., Belton, M.J.S., and the Galileo Imaging Team, 1998: The Shape of Io from Galileo Limb Measurements. Icarus 135, 175–180.

Thomas, P.C., Burns, J.A., Helfenstein, P., Squyres, S., Veverka, J., Porco, C.C., Turtle, E.P., McEwen, A., Denk, T., Giese, B., Roatsch, T., Johnson, T.V., and Jacobson, R.A., 2007: Shapes of the Saturnian icy satellites and their significance. Icarus 179, 573–584.